Journal of Sound and Vibration (2002) **250**(4), 627–648
doi:10.1006/jsvi.2001.3956, available online at http://www.idealibrary.com on IDEAL®

AN INVESTIGATION OF POWER FLOW CHARACTERISTICS OF L-SHAPED PLATES ADOPTING A SUBSTRUCTURE APPROACH

Z. H. Wang, J. T. Xing and W. G. Price

School of Engineering Sciences, Ship Science, University of Southampton, Southampton SO17 1BJ, England. E-mail: jtxing@soton.ac.uk

(*Received* 1 *May* 2001, *and in final form* 18 *July* 2001)

A substructure approach with free–free interface condition is formulated to investigate the power flow characteristics of an L-shaped plate. This is achieved by complementing the normal dynamic equations with geometric compatibility equations allowing the assessment of power flow dynamic characteristics applied to and excited within the system. The displacement contribution of the external and boundary coupling forces is deduced, permitting determination of the power flow between the interfaces of substructures. A power flow density vector is defined and the corresponding power flow lines illustrate the flow of power in the plate. Numerical examples demonstrate the applicability of the method and detailed configurations display the power flow characteristics associated with L-shaped plates. The proposed method can calculate the higher modes easily and efficiently to ensure convergence of solution as well as readily taking into account variations in substructure damping.

1. INTRODUCTION

In the low-frequency range, the dynamic behaviour of a structure is normally derived through deterministic methods such as the finite element method (FEM). In the high-frequency range where high modal densities are experienced, the response of the system is sensitive to small details of construction, properties and boundary conditions, once the wavelength is comparable to the dimensions of the details which are not always known with sufficient accuracy. Energy-based approaches such as a statistical energy analysis (SEA) [1] and/or a power flow analysis (PFA) are therefore adopted. The SEA approach provides only the global space-averaged information of the field variables with the loss of detailed knowledge of the local distribution of the variables. In contrast, the PFA approach is applicable over all frequency ranges and the parameters of power flow and mobility may be expressed as an aggregate of modal functions to retain the resonant behaviour of the individual and global structures at low modal density. If it is assumed that all phase effects may be neglected at high modal density, the mobilities or vibrational energy can be described in a similar form to those obtained by SEA [2, 3].

The fundamental concepts of power flow analysis, as discussed and described by Goyder and White [4–6], use the rate of energy flow to characterize the dynamic response of vibrating systems. Several PFA approaches have been presented which combine the theoretical solution of individual structural elements. These include the mobility approach applied to an L-shaped plate by Cuschieri [7], the direct dynamic stiffness method in

0022-460X/02/090627 + 22 $35.00/0

a general frame of reference by Langley [8], the travelling and scattering wave approach to a beam frame by Miller and Flotow [9], Horner and White [10], Beale and Accorsi [11], the progressive approaches to coupled systems by Xiong *et al.* [12], the substructure receptance approach in an indeterminate beam system by Wang *et al.* [13], and in two coupled rectangular plates by Farag and Pan [14], Beshara and Keane [15]. The general objective of these studies [7–15] is to assess the total power flow across the coupling edges and joints of the subsystems.

A power flow finite element method was proposed by Nefske and Sung [16] and investigated by Wohlever and Bernhard [17]. This method is based on a heat conduction analogy with mechanical power flow and the latter authors showed that this analogy is only approximately true for rods and beams.

Applications of FEA to energy flow modelling are described by Simmons [18], Stimpson and Lalor [19], Steel and Craik [20], Fredo [21] and Mace and Shorter [22]. These authors express the response of a finite element model in terms of an energy flow through a global finite element analysis performed on a global system. Shankar and Keane [23, 24] develop an alternative local FEA method using a receptance approach in which the response of each subsystem is described by a Green function to analyze energy flow for both simple and complex models. These FEA studies focus on the relation between FEA and SEA by calculating the kinetic energy of the system.

Hambric [25] and Gavric and Pavic [26] use FEA to calculate structural intensities. It is advantageous to use FEA models in a power flow analysis and in structural intensity calculations because they can be conveniently applied to complex structures subject to boundary conditions. However, in general, because the structural intensity prediction requires an accurate description of various spatial derivatives and it is necessary to admit a large number of modes into the analysis to ensure convergence of solution, a numerical approach adopting modal superposition encounters difficulties due to the computational effort required. To ease this problem, Xing and Price [27] developed the concept of an energy flow density vector which uniquely defines the energy transmission between one part of a system and another. The analysis of structural intensity or energy flow density vector identifies the magnitude and direction of the power at any location in a structure and allows the determination of dominant paths of energy flow. An understanding of the mechanisms and paths of energy transmission flowing from a vibration source to other parts of a structure has been recognized as an important tool to control vibration [28].

This paper examines the power flowing in an L-shaped plate system excited by an external force (see, Figure 1). A theoretical modal substructure approach is used to evaluate the vibrational power flow between plates and the power flow density (or structural intensity) in two plates. Hence, natural frequencies and principal mode shapes of a rectangular plate are first determined and then a receptance function derived for the coupled plate system. According to thin plate theory (see, reference [29]), the assumptions of small deflections and small slopes of the shapes lead to an equation governing the bending vibration which is uncoupled to the in-plane vibration. When two or more plates are coupled at a non-zero angle, the bending vibration of one plate couples with the in-plane vibration of the other even when only a lateral load is applied. The receptance function of the plate structure used herein therefore neglects the coupling between bending and in-plane vibrations but they are coupled at the junction of the two plates. The aim of this study is to examine as to how power flows within and across the plates to determine the power flow characteristics in coupled plate structures. The main advantage of this approach is an ability to calculate the higher modes easily and efficiently as well as readily taking into account variations in substructure damping but it has a limitation, namely, the receptance function of the substructure can only be achieved analytically.

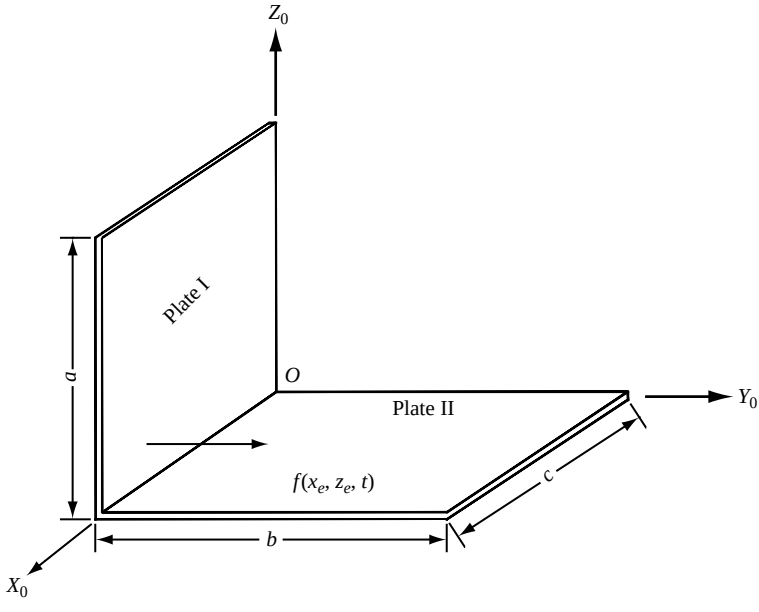

Figure 1. Schematic illustration of an L-shaped plate system.

2. SUBSTRUCTURE APPROACH TO AN L-SHAPED PLATE

2.1. THE COUPLING OF SUBSYSTEMS

The L-shaped plate system under investigation is illustrated in Figure 1. It is assumed that simply supported boundary conditions apply on the plate edges except on the forcing or coupling edge. This total system can be separated into two subsystems with each subsystem under examination as shown in Figure 2. That is, a rectangular plate with simply supported boundary conditions applied to three edges of the plate with the coupling edge ($y = b$) assumed free.

Two kinds of forces act on the plate. One is the external excitation force at position (x_e, y_e) whereas the other is the internal distributed coupling force acting at the coupling edge, see Figure 2. The whole system is coupled at the coupling edge by the distributed internal forces of bending moment M_{yy}, transverse shear force Q_y and in-plane longitudinal force N_{yy} along the free edge of each subsystem. The internal force vector $[\mathbf{f}^c] = [N_{yy}, Q_y, M_{yy}]^T$ and relative displacement vector $[\mathbf{U}^c] = [w_y, w, \theta_x]^T$ at the coupling edge in the local co-ordinate axis reference system (X, Y, Z) are related to those in the global co-ordinate (X_0, Y_0, Z_0) by an orthogonal transformation matrix $[\mathbf{T}]$ (see, for example, reference [30]) expressed as

$$[\mathbf{f}_0^c] = [\mathbf{T}][\mathbf{f}^c], \qquad [\mathbf{U}_0^c] = [\mathbf{T}][\mathbf{U}^c], \tag{1}$$

where

$$[\mathbf{T}] = \begin{bmatrix} \cos\alpha & -\sin\alpha & 0 \\ \sin\alpha & \cos\alpha & 0 \\ 0 & 0 & 1 \end{bmatrix}. \tag{2}$$

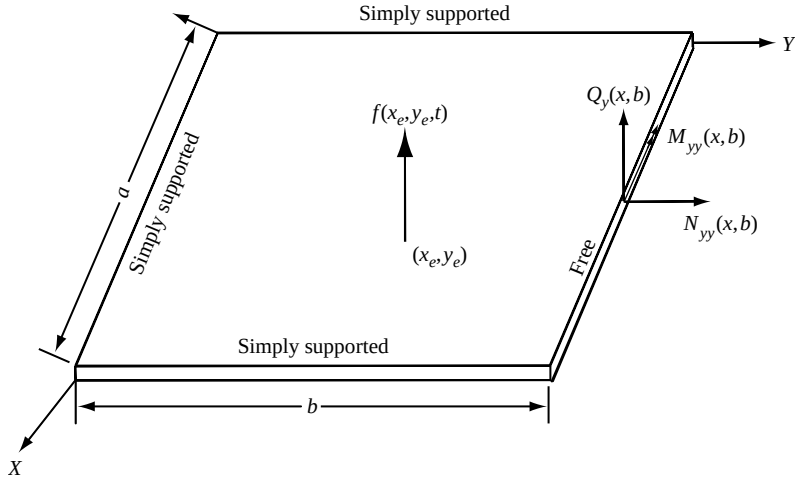

Figure 2. Schematic illustration of a subsystem in the local co-ordinate system.

The coupling relationship between two connected plates is expressed by their force balance and geometric compatible conditions at the coupling edge in the global co-ordinate system. For example, for the jth and kth plates at a coupling edge shown in Figure 2, the respective coupling relationships are given by force balance and geometrically compatible conditions as

$$[\mathbf{T}_j][\mathbf{U}_j^c] = [\mathbf{T}_k][\mathbf{U}_k^c], \tag{3}$$

$$[\mathbf{T}_j][\mathbf{f}_j^c] + [\mathbf{T}_k][\mathbf{f}_k^c] = 0, \quad j, k = 1, 2;\ j \neq k. \tag{4}$$

The displacement vectors at the coupling edges can be further expressed in terms of components excited by an external excitation vector $[\mathbf{f}^e]$ and an internal coupling force vector $[\mathbf{f}^c]$. For example, the displacement vector on the jth plate is given by

$$[\mathbf{U}_j^c] = [\mathbf{M}b_j^e][\mathbf{f}_j^e] + [\mathbf{M}b_j^c][\mathbf{f}_j^c], \quad j = 1, 2. \tag{5}$$

Equation (4) can be rewritten as

$$[\mathbf{f}_k^c] = -[\mathbf{T}_k]^{-1}[\mathbf{T}_j][\mathbf{f}_j^c]. \tag{6}$$

Substituting equations (5, 6) into equation (3), the coupling forces are expressed in the form

$$[\mathbf{f}_j^c] = ([\mathbf{T}_k][\mathbf{M}b_k^c][\mathbf{T}_k]^{-1}[\mathbf{T}_j] + [\mathbf{T}_j][\mathbf{M}b_j^c])^{-1}\{[\mathbf{T}_k][\mathbf{M}b_k^e][\mathbf{f}_k^e] - [\mathbf{T}_j][\mathbf{M}b_j^e][\mathbf{f}_j^e]\}. \tag{7}$$

It therefore follows that the response of the plate system can be determined after the solution of the receptance function of a single rectangular plate. If it is assumed that the coupling edge between the two plates is simply supported, the coupling relationship simplifies to

$$\theta_{xj} = \theta_{xk}, \qquad M_{yyj} + M_{yyk} = 0. \tag{8}$$

This formula is independent of the coupling angle α. The coupling relation presented here is derived in a general manner, so it can be applied to any coupling angle α and to a more complex joined plate structure.

2.2. BENDING VIBRATION OF A SUBSYSTEM

As shown in Figure 2, each subsystem is treated as an idealized system consisting of a single rectangular uniform plate simply supported at three edges with a free edge at $y = b$. Its structural damping properties are represented by a linear Voigt viscoelastic model with hysteretic damping or loss factor η. A harmonic external exciting force is applied at (x_e, y_e) and internal distributed coupling forces act on the free edge of the plate.

Under the assumptions of thin plate theory (see, for example, reference [29]), the differential equation describing plate bending vibration is expressed as

$$\rho h\ddot{w}(x, y, t) + D\nabla^4 w(x, y, t) = f(x, y, t)\,\delta(x - x_e)\,\delta(y - y_e), \tag{9}$$

where

$$D = Eh^3/12(1 - \mu^2), \tag{10}$$

with stress–displacement relations

$$M_{xx} = -D(\partial^2 w/\partial x^2 + \mu\,\partial^2 w/\partial y^2), \qquad M_{yy} = -D(\partial^2 w/\partial y^2 + \mu\,\partial^2 w/\partial x^2),$$

$$M_{xy} = M_{yx} = -D(1 - \mu)\,\partial^2 w/\partial x \partial y, \tag{11}$$

$$Q_x = -D(\partial^3 w/\partial x^3 + \partial^3 w/\partial x \partial y^2), \qquad Q_y = -D(\partial^3 w/\partial y^3 + \partial^3 w/\partial x^2 \partial y). \tag{12}$$

The solutions of natural frequencies and principal mode shapes of a rectangular plate under different boundary conditions are given by Leissa [29] and Gorman [31] based on a Levy-type solution. A finite element analysis is also a very useful technique to derive the natural frequencies and principal mode shapes of a rectangular plate as discussed in references [23, 24].

For a rectangular plate simply supported at three edges and free at the fourth edge, the eigenvalue equation and relative principal mode shapes are given by [31]

$$\gamma_r(\gamma_r^2 + (2 - \mu)\phi^2 r^2\pi^2)(\beta_r^2 - \mu\phi^2 r^2\pi^2)\sinh\beta_r\cos\gamma_r$$
$$= \beta_r(\beta_r^2 - (2 - \mu)\phi^2 r^2\pi^2)(\gamma_r^2 + \mu\phi^2 r^2\pi^2)\cosh\beta_r\sin\gamma_r, \tag{13a}$$

$$\varphi_r(x, y) = \left[\sin\frac{\gamma_r y}{b} + \frac{(\gamma_r^2 + \mu\phi^2 r^2\pi^2)\sin\gamma_r}{(\beta_r^2 - \mu\phi^2 r^2\pi^2)\sinh\beta_r}\sinh\frac{\beta_r y}{b}\right]\sin\frac{r\pi x}{a}, \tag{13b}$$

for $\lambda_r > r\pi$, $r = 1, 2, 3, \ldots$, or

$$\gamma_r(\gamma_r^2 - (2 - \mu)\phi^2 r^2\pi^2)(\beta_r^2 - \mu\phi^2 r^2\pi^2)\sinh\beta_r\cosh\gamma_r$$
$$= \beta_r(\beta_r^2 - (2 - \mu)\phi^2 r^2\pi^2)(\gamma_r^2 - \mu\phi^2 r^2\pi^2)\cosh\beta_r\sinh\gamma_r, \tag{14a}$$

$$\varphi_r(x, y) = \left[\sinh\frac{\gamma_r y}{b} - \frac{(\gamma_r^2 - \mu\phi^2 r^2\pi^2)\sinh\gamma_r}{(\beta_r^2 - \mu\phi^2 r^2\pi^2)\sinh\beta_r}\sinh\frac{\beta_r y}{b}\right]\sin\frac{r\pi x}{a}, \tag{14b}$$

for $\lambda_r \leqslant r\pi$, where $\gamma_r = \phi\sqrt{|\lambda_r^2 - (r\pi)^2|}$, $\beta_r = \phi\sqrt{\lambda_r^2 + (r\pi)^2}$.

For any r ($= 1, 2, 3, \ldots$), a solution of the natural frequency $\omega_{rp} = (\lambda_{rp}^2/a^2)\sqrt{D/\rho}$ ($p = 1, 2, 3, \ldots$) is obtained numerically from eigenvalue equation (13a) or (14a). Its relative principal mode shape $\varphi_{rp}(x, y)$ is determined using equation (13b) or (14b).

According to a theorem given by Rayleigh [32], any distortion of the plate may be expressed as an aggregate of distortions in its principal modes. That is,

$$w(x, y, t) = \sum_{r=1}^{n}\sum_{p=1}^{m}\varphi_{rp}(x, y)P_{rp}(t). \tag{15}$$

The principal co-ordinate of the plate under examination (see, for example, reference [33]) is given by

$$P_{rp}(t) = \frac{\mathbf{f}(x_e, y_e)\varphi_{rp}(x_e, y_e) + \int_0^a [Q_y(x, b)\varphi_{rp}(x, b) + M_{yy}(x, b)\varphi'_{rp}(x, b)]\,\mathrm{d}x}{m_{rp}[\omega_{rp}^2 - \omega^2 + \mathrm{i}\omega_{rp}^2\eta]}\,\mathrm{e}^{\mathrm{i}\omega t}. \tag{16}$$

Thus, the displacement of the rectangular plate is expressed as

$$w(x, y, t) = \sum_{r=1}^{n}\sum_{p=1}^{m} \varphi_{rp}(x, y)\frac{\mathbf{f}(x_e, y_e)\varphi_{rp}(x_e, y_e) + \int_0^a [Q_y(x, b)\varphi_{rp}(x, b) + M_{yy}(x, b)\varphi'_{rp}(x, b)]\,\mathrm{d}x}{m_{rp}[\omega_{rp}^2 - \omega^2 + \mathrm{i}\omega_{rp}^2\eta]}\,\mathrm{e}^{\mathrm{i}\omega t} \tag{17}$$

with the rotation angles,

$$\theta_x(x, y, t) = \frac{\partial w(x, y, t)}{\partial y} = \sum_{r=1}^{n}\sum_{p=1}^{m} \frac{\partial \varphi_{rp}(x, y)}{\partial y} P_{rp}(t), \tag{18}$$

$$\theta_y(x, y, t) = \frac{\partial w(x, y, t)}{\partial x} = \sum_{r=1}^{n}\sum_{p=1}^{m} \frac{\partial \varphi_{rp}(x, y)}{\partial x} P_{rp}(t). \tag{19}$$

Equations (17–19) describe the relationship between the general displacement responses $\mathbf{U}(x, y, t)$ and excitations. That is, the receptance function which, in matrix form, can be written as

$$\{\mathbf{U}(x, y, t)\} = [\mathbf{M}b^e(x, y, x_e, y_e)]\{\mathbf{f}(x_e, y_e)\mathrm{e}^{\mathrm{i}\omega t}\} + [\mathbf{M}b^c(x, y, x_c, b)]\{\mathbf{f}^c(x_c, b)\mathrm{e}^{\mathrm{i}\omega t}\}. \tag{20}$$

It is noted that all the receptance matrixes and internal forces $\mathbf{f}^c(x_c, b)$ have complex value elements due to the influence of damping.

2.3. IN-PLANE VIBRATION OF A THIN RECTANGULAR PLATE

The basic underlying assumption of in-plane vibration of a rectangular plate lies in the fact that a small deflection and small slope in the deformed shape leads to a bending vibration in the plate which is uncoupled from the in-plane vibration. The differential equations describing in-plane vibration of a plate (see, for example, reference [29]) under excitation force vector $[\mathbf{f}_x, \mathbf{f}_y]\,\mathrm{e}^{\mathrm{i}\omega t}$ at position (x_e, y_e) are given by

$$C_L^2\frac{\partial^2 w_x}{\partial x^2} + C_T^2\frac{\partial^2 w_x}{\partial y^2} + (\mu C_L^2 + C_T^2)\frac{\partial^2 w_y}{\partial x \partial y} + \omega^2 w_x = -\frac{\mathbf{f}_x}{\rho h}\delta(x - x_e)\delta(y - y_e), \tag{21}$$

$$C_L^2\frac{\partial^2 w_y}{\partial y^2} + C_T^2\frac{\partial^2 w_y}{\partial x^2} + (\mu C_L^2 + C_T^2)\frac{\partial^2 w_x}{\partial x \partial y} + \omega^2 w_y = -\frac{\mathbf{f}_y}{\rho h}\delta(x - x_e)\delta(y - y_e). \tag{22}$$

Theoretical solutions of equations (21, 22) are difficult to derive analytically because these two equations are coupled. Numerical methods, for example FEA, can be used to obtain accurate solutions for the in-plane vibration of the plate under different boundary conditions (see, reference [34]). Langley [8], Farag and Pan [14] resort to an approximate method for simple engineering applications. They assume neglect of the coupling between displacement responses w_x and w_y resulting in the absence of the third term on the left hand

side of equations (21, 22). The coupling between w_x and w_y is due to the Poisson effects and shear waves accompanying the longitudinal waves. The main emphasis of the present study is to assess the coupling between longitudinal and flexural vibrations of the plates at the coupling edge, so it is reasonable to neglect the influences of the Poisson effects and shear waves in the manner of Farag and Pan [14]. When the plate is assumed clamped at $x = 0$, $x = a$, $y = 0$ and free at $y = b$, the solution of equation (22) takes the form

$$w_y(x, y, t) \approx \sum_{r=1}^{n} \sum_{p=1,3,5,\ldots}^{m} A_{rp} \sin \frac{r\pi x}{a} \sin \frac{p\pi y}{2b} e^{i\omega t}. \tag{23}$$

The governing equation for in-plane vibration becomes

$$\sum_{r=1}^{n} \sum_{p=1,3,\ldots,}^{m} \left\{ C_L^2 \left(\frac{p\pi}{2b}\right)^2 + C_T^2 \left(\frac{r\pi}{a}\right)^2 - \omega^2 \right\} \sin \frac{r\pi x}{a} \sin \frac{p\pi y}{2b} A_{rp}$$

$$= \frac{\mathbf{f}_y}{\rho h} \delta(x - x_e)\delta(y - y_e) \tag{24}$$

and after using the orthogonal property of the assumed principal mode shapes,

$$A_{rp} = \frac{4\mathbf{f}_y \sin (r\pi x_e/a) \sin p\pi y_e/2b}{\rho abh[C_L^2(r\pi/a)^2 + C_T^2(p\pi/2b)^2 - \omega^2]} \tag{25}$$

for $r = 1, 2, 3, \ldots, n$ and $p = 1, 3, 5, \ldots, m$.

The displacement response w_x in the x direction has the same form as described in equations (23, 25). These solutions can be expressed in a receptance matrix form similar to equation (20).

The internal forces per unit width caused by in-plane vibration are given by

$$N_{xx} = \frac{-Eh}{1-\mu^2}\left(\frac{\partial w_x}{\partial x} + \mu \frac{\partial w_y}{\partial y}\right), \qquad N_{yy} = \frac{-Eh}{1-\mu^2}\left(\frac{\partial w_y}{\partial y} + \mu \frac{\partial w_x}{\partial x}\right),$$

$$N_{xy} = N_{yx} = \frac{-Eh}{2(1+\mu)}\left(\frac{\partial w_x}{\partial y} + \frac{\partial w_y}{\partial x}\right) \tag{26}$$

and are determined knowing w_x and w_y.

3. POWER FLOW CHARACTERISTICS IN AN L-SHAPED PLATE

3.1. POWER FLOW DENSITY VECTOR

The instantaneous power flow density vector in a continuum introduced by Xing and Price [27] is defined by the dot product of the velocity vector v_j and stress tensor $\boldsymbol{\sigma}_{jk}$ given by

$$q_k = -\operatorname{Re}\{v_j\} \operatorname{Re}\{\boldsymbol{\sigma}_{jk}\}, \; j, \; k = 1, 2, 3, \tag{27}$$

where a standard Cartesian tensor notation and a summation convention are used. This power flow density vector specifies the energy transmitted from one part of a dynamic system to another per unit time and allows the determination of power flow at each point in or on the continuum in any direction. Its time-averaged quantity over a period of

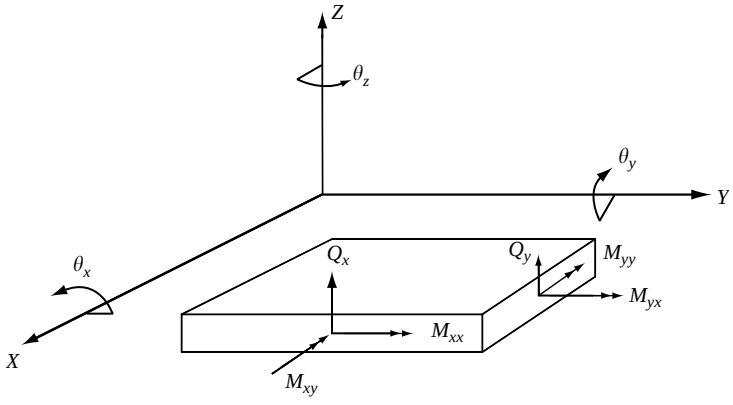

Figure 3. Direction convention of force and displacement components on a plate element.

excitation T is

$$\langle q_k \rangle = \frac{1}{T}\int_0^T q_k \, \mathrm{d}t = -\tfrac{1}{2}\,\mathrm{Re}\{\boldsymbol{\sigma}_{kj} v_j^*\}. \tag{28}$$

The time-averaged power flow density vector$\langle q_k \rangle$ in equation (28) is equivalent to the structural intensity parameter described elsewhere [25, 26] and is similar to an acoustic intensity parameter in a fluid domain being the product of pressure and the in-phase component of fluid particle velocity (see, for example, reference [35]).

The instantaneous power flow density vector in a thin plate (see, for example, reference [27]) is defined as

$$q_k = -\,\mathrm{Re}\{v\}\,\mathrm{Re}\{Q_k\} + \mathrm{Re}\{v_{,j}\}\,\mathrm{Re}\{M_{jk}\} - \mathrm{Re}\{\dot{w}_j\}\,\mathrm{Re}\{N_{jk}\}, \tag{29}$$

where $j = 1, 2 = k$. The sign of the second term on the right-hand side of equation (29) is dependent on the direction definitions of $\dot{\theta}_j$ and M_{jk}. They are defined in Figure 3 based on the sign convention of elasticity theory (see, for example, reference [30]).

The time-averaged power flow density vector over a period of excitation in the thin plate is

$$\langle q_k \rangle = -\tfrac{1}{2}\,\mathrm{Re}\{Q_k v^* - M_{kj} v_{,j}^* + N_{kj}\dot{w}_k^*\}. \tag{30}$$

When the plate is simply supported at all edges and only transverse exciting forces exist, the component of in-plane vibration in equations (29, 30), i.e. $\mathrm{Re}\{\dot{w}_j\}\,\mathrm{Re}\{N_{jk}\}$ or $\mathrm{Re}\{N_{kj}\dot{w}_k^*\}$, is equal to zero.

The instantaneous power flow density vector in the coupling edge is only in the y direction (see, Figure 2) and can be expressed as

$$\begin{aligned} q_y^c = &-\mathrm{Re}\{v\}\,\mathrm{Re}\{Q_y\} + \mathrm{Re}\{\dot{\theta}_y\}\,\mathrm{Re}\{M_{xy}\} + \mathrm{Re}\{\dot{\theta}_x\}\,\mathrm{Re}\{M_{yy}\} \\ &-\mathrm{Re}\{\dot{w}_x\}\,\mathrm{Re}\{N_{xy}\} - \mathrm{Re}\{\dot{w}_y\}\,\mathrm{Re}\{N_{yy}\}, \end{aligned} \tag{31}$$

with a time-averaged quantity,

$$\langle q_y^c \rangle = -\,\tfrac{1}{2}\,\mathrm{Re}\{Q_y v^* + N_{xy}\dot{w}_x^* + N_{yy}\dot{w}_y^* - M_{xy}\dot{\theta}_y^* - M_{yy}\dot{\theta}_x^*\}. \tag{32}$$

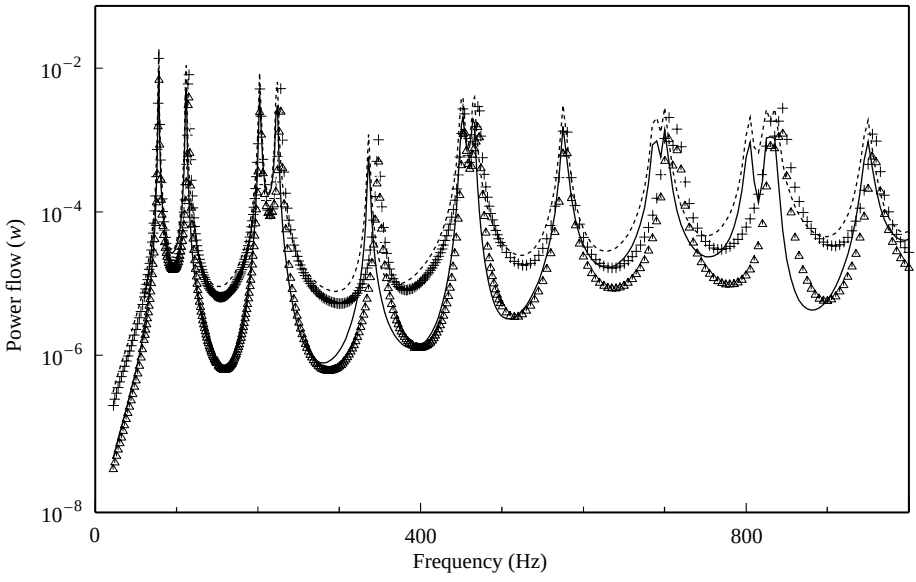

Figure 4. Results of time-averaged input power and transmitted power flows (excitation at the centre of plate I): $+$, input power (FEA); $\triangle$, transmitted power (FEA); – – –, input power; —, transmitted power.

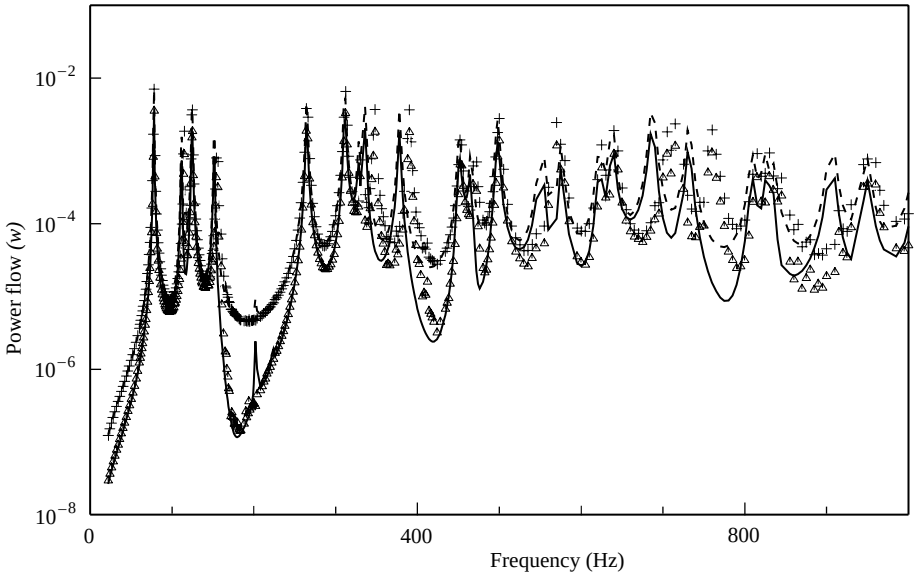

Figure 5. Results of time-averaged input power and transmitted power flows (excitation at $x_e = 0{\cdot}33$ m, $y_e = 0{\cdot}125$ m of plate I): $+$, input power (FEA); $\triangle$, transmitted power (FEA); – – –, input power; —, transmitted power.

If the boundary condition on the coupling edge in Figure 2 is also simply supported, equations (31, 32) become

$$q_k^c = \mathrm{Re}\{\dot{\theta}_x\}\,\mathrm{Re}\{M_{yy}\}, \qquad \langle q_k^c \rangle = \tfrac{1}{2}\,\mathrm{Re}\{M_{yy}\dot{\theta}_x^*\}. \tag{33, 34}$$

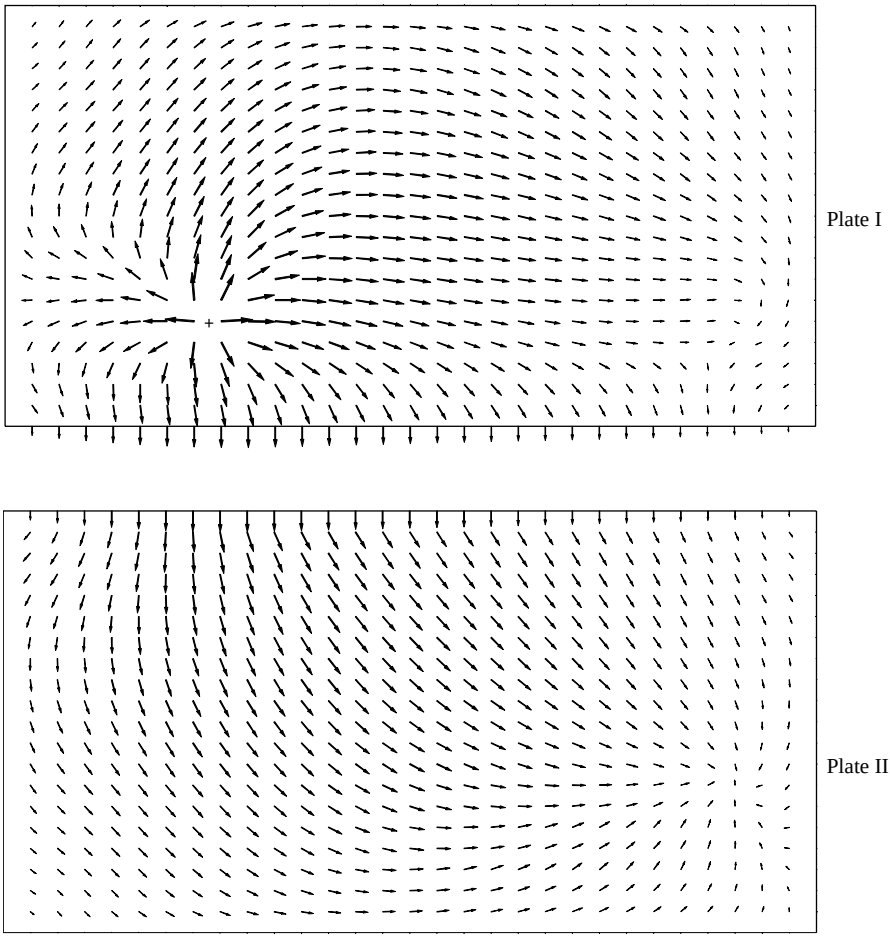

Figure 6. Time-averaged power flow density vector in two plates, $f = 77{\cdot}7$ Hz. " + " indicates the excitation position.

The total transmitted power in a coupling edge is given by the integral of the transmitted power flow density along the length of the coupling edge. That is,

$$q_{trans} = \int_0^a q_y^c \, \mathrm{d}x \tag{35}$$

with corresponding time-averaged quantity,

$$\langle q_{trans} \rangle = \int_0^a \langle q_y^c \rangle \, \mathrm{d}x. \tag{36}$$

It is convenient to determine the power flow at the coupling edge using a substructure receptance approach because the solution of the coupling force $[\mathbf{f}_j^c]$ in the coupling relationship equations (6, 7) and the receptance function expressed in equation (20) is simple and in the same local co-ordinate axis system.

If an external exciting force $|\mathbf{f}|\mathrm{e}^{\mathrm{i}\omega t}$ is applied at position (x_e, y_e) and the velocity response at this position is $v_e\mathrm{e}^{\mathrm{i}\omega t} = |v_e|\mathrm{e}^{\mathrm{i}(\omega t + \varphi_v)}$, the input power from this excitation is given

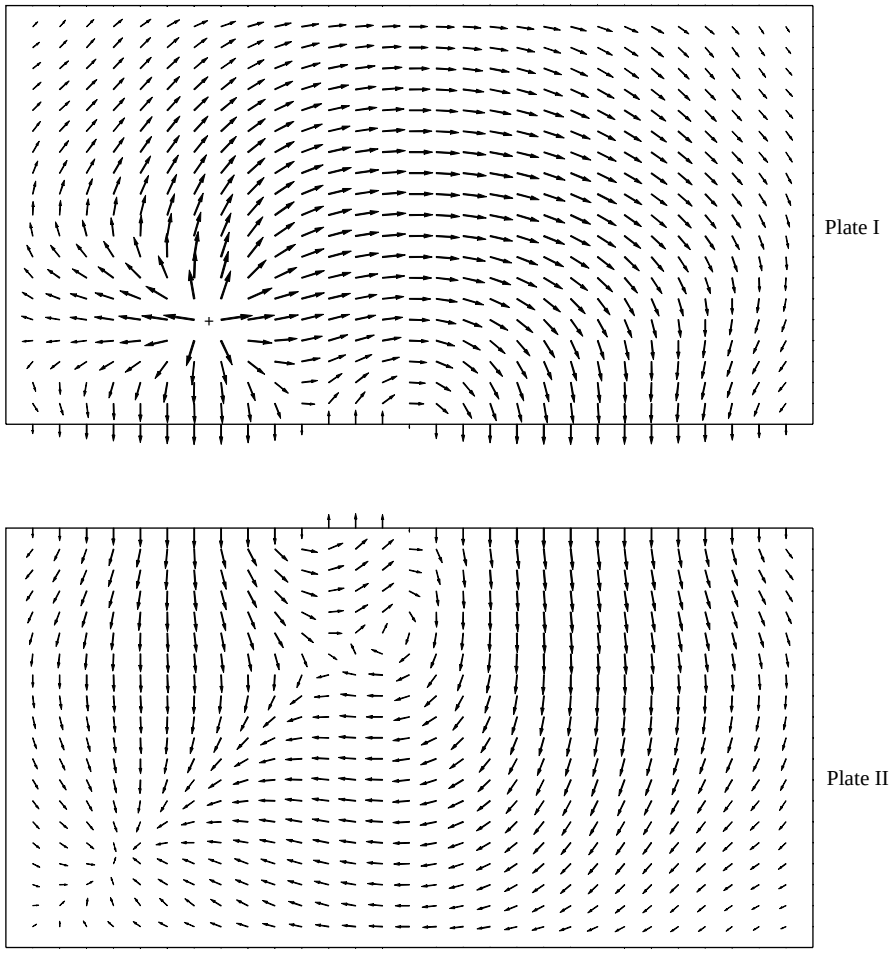

Figure 7. Time-averaged power flow density vector in two plates, $f = 124{\cdot}1$ Hz. " + " indicates the excitation position.

by

$$q_{in}(t) = \mathrm{Re}\{|\mathbf{f}|e^{i\omega t}\}\ \mathrm{Re}\{v_e e^{i\omega t}\} = \tfrac{1}{2}|\mathbf{f}| \cdot |v_e| \cdot [\cos\varphi_v + \cos(2\omega t + \varphi_v)] \tag{37}$$

with corresponding time-averaged quantity,

$$\langle q_{in}(t)\rangle = \tfrac{1}{2}|\mathbf{f}| \cdot |v_e| \cos\varphi_v. \tag{38}$$

3.2. CALCULATION EXAMPLE

For illustrative purposes, one assumes that the L-shaped plate system shown in Figure 1 is defined by the data set: $\rho = 2710\ \mathrm{kg/m^3}$, $E = 72$ GPa, $\eta = 0{\cdot}01$, $\mu = 0{\cdot}3$; $a = b = 0{\cdot}5$ m, $c = 1{\cdot}0$ m, $h = 0{\cdot}00635$ m.

Two coupling edge conditions were examined. The first assumes that simply supported boundary conditions apply at all edges of each plate including the coupling edge. This system was originally examined by Cuschieri [7] to assess the power flow transmitted

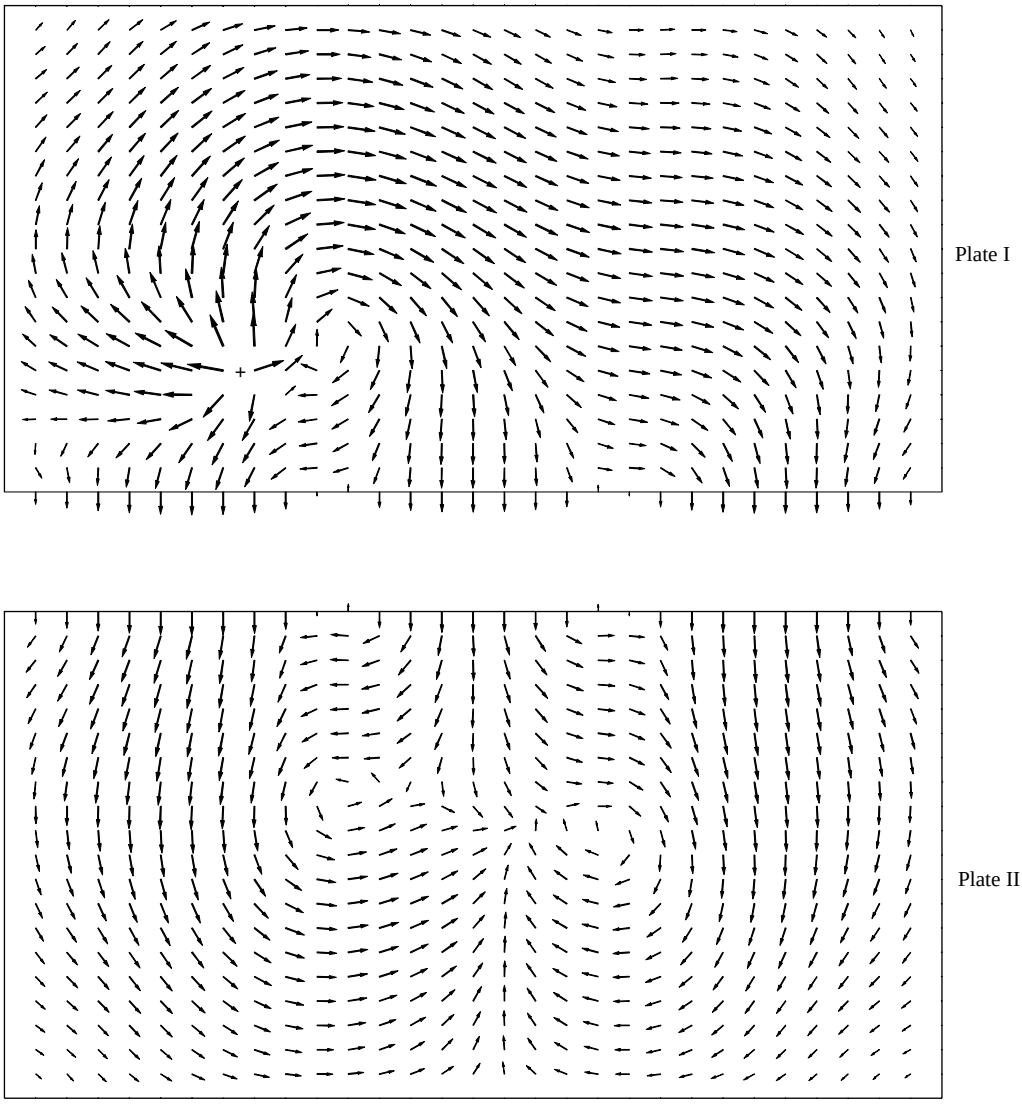

Figure 8. Time-averaged power flow density vector in two plates, $f = 201{\cdot}4$ Hz. " + " indicates the excitation position.

between two plates adopting a mobility function approach. The other assumes that simply supported boundary conditions apply at three edges of each plate but the plates are rigidly connected at the coupling edge. More complex boundary conditions may be adopted, e.g., fixed or free at some edges of a plate, etc., which complicates the analysis without contributing significant additional insights into the power flow mechanism occurring in the coupled plate system.

3.2.1. *Simply supported coupling edge*

Figures 4 and 5 illustrate the variation of the time-averaged input power and transmitted power flows with frequency to an amplitude loading applied at different positions. Figure 4

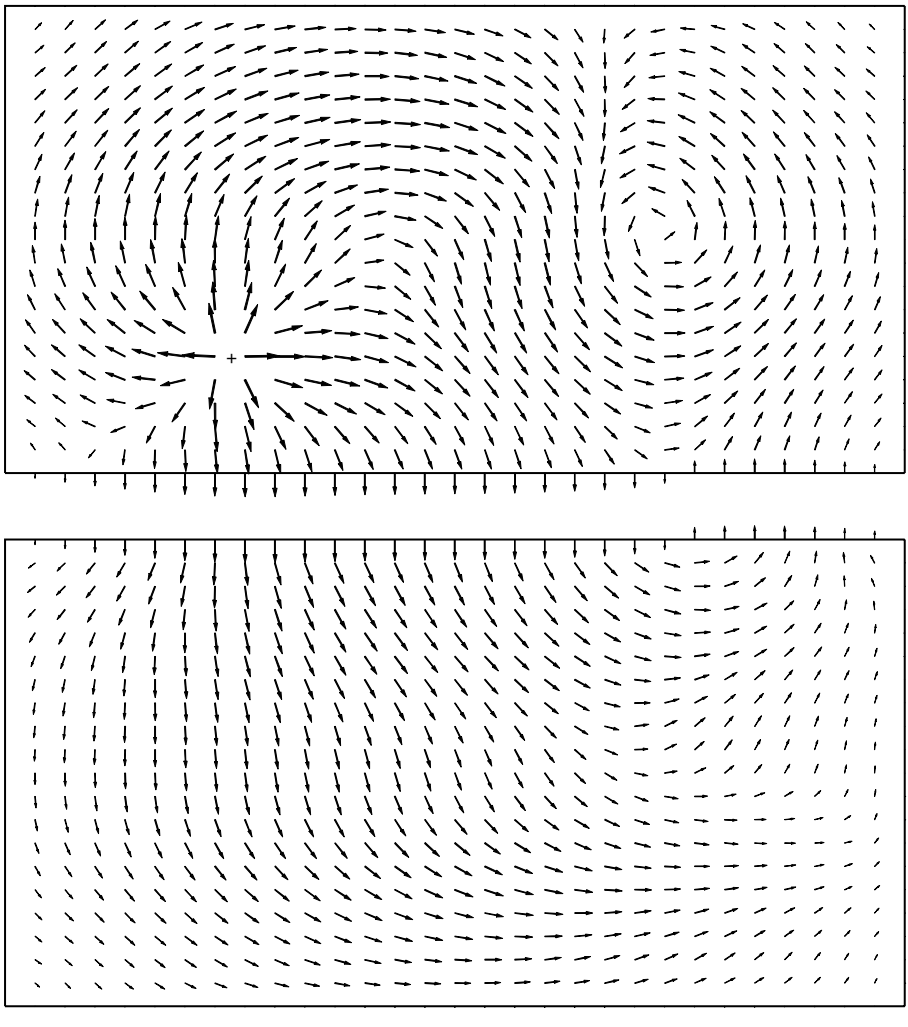

Figure 9. Time-averaged power flow density vector in two plates, $f = 263{\cdot}8$ Hz. " + " indicates the excitation position.

shows the results of an excitation at the centre of plate I, whereas Figure 5 displays the predictions caused by a loading at position (0·33 m, 0·125 m) on plate I. The calculated time-averaged transmitted power flow values at the coupling edge demonstrate the same trends and magnitudes as those presented by Cuschieri [7]. The receiving plate, i.e., plate II in Figure 2 is not connected to any other substructure except the source plate (plate I), and thus the transmitted time-averaged power in Figures 4 and 5 equals the rate of energy dissipation due to the internal loss factor. The total energy dissipation of the system in a period is equal to the time averaged input power in Figures 4 and 5.

Because receptance functions of many practical engineering structures cannot be determined theoretically, the results derived by an FEA substructure receptance approach are also included in Figures 4 and 5. The FEA plate model has the same structural characteristics as the original substructure and contains 527 nodes and 480 plate–shell

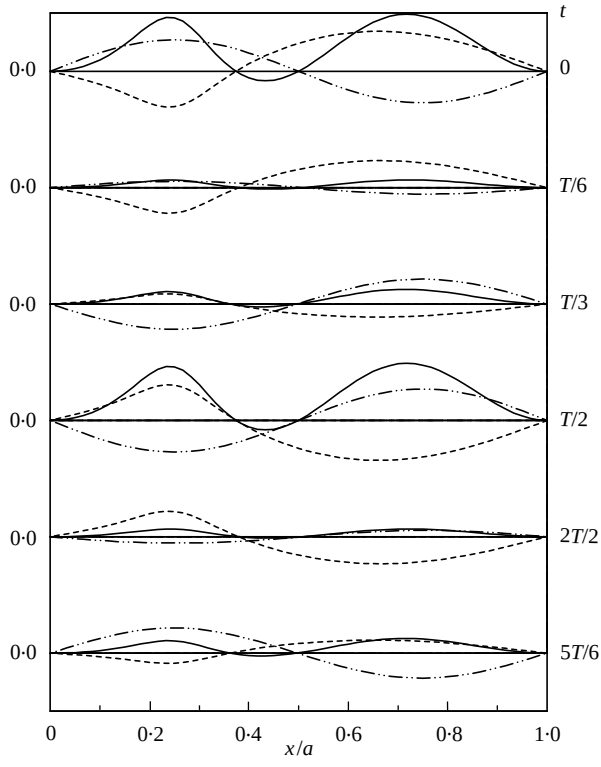

Figure 10. Shapes of instantaneous bending moment, angular velocity and transmitted power flow along the coupling edge of plate I at a frequency of 124·1 Hz: – – –, angular velocity; – – – –, bending moment; ——, instantaneous power.

elements. Ninety natural frequencies and principal mode shapes of a plate were extracted using FEA package ANSYS spanning the frequency range up to 4150 Hz. It is observed that only small differences exist between the theoretical substructure predictions and those evaluated by the FEA approach after 500 Hz as illustrated in Figures 4 and 5. This is because only a small number of principal mode shapes are used in the FEA substructure approach (see, for example, reference [36]). At approximately 200 Hz in Figure 5, there exists a small peak in the analytical approach which does not appear in the FEA solution. In the analytical model, the excitation is positioned at (0·33, 0·125) which because of the automatic modelling process of ANSYS approximates to (0·3333, 0·125). This latter position falls on the node line of the mode with a natural frequency of about 200 Hz. The analytical calculation was repeated at (0·3333, 0·125) and these results showed similar trends to those derived numerically.

In the following presentation of spatial distributions of time-averaged power flow density vectors, Figures 6–9 relate to a unit amplitude exciting force applied at position $x_e = 0{\cdot}75$ m, $y_e = 0{\cdot}125$ m on plate I and this position of excitation is indicated by the symbol " + " in these figures. For clarity of presentation, the modulus of time-averaged power flow density vectors in Figures 6–9 are defined as

$$|\langle q(x, y)\rangle|^{(d)} = |\langle q(x, y)\rangle|^{0{\cdot}2} = (|q_x(x, y)|^2 + |q_y(x, y)|^2)^{0{\cdot}1}. \tag{39}$$

Figure 6 illustrates the distribution of the time-averaged power flow density vector at a frequency of 77·7 Hz. This corresponds to the first natural frequency of the system with

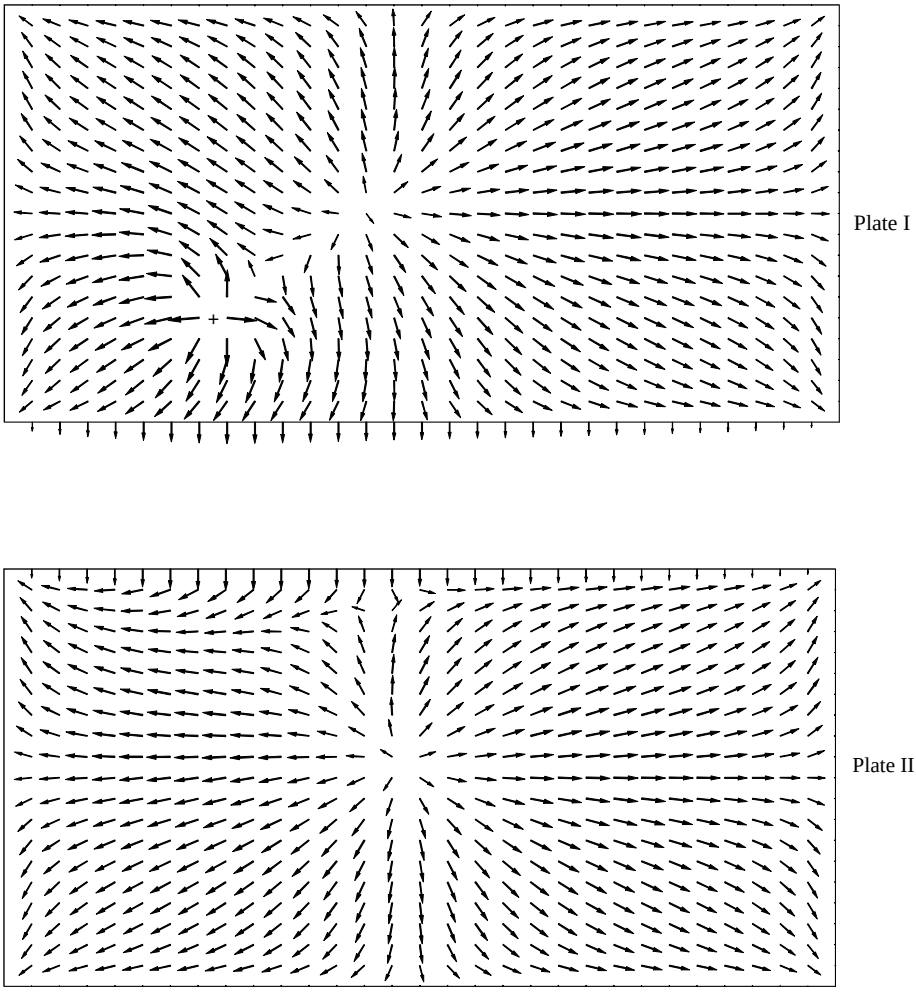

Figure 11. Instantaneous power flow density vector at $f = 77{\cdot}7$ Hz, $t = 0$. " + " indicates the excitation position.

one bending wave in both x and y directions in each plate. Figure 7 shows the corresponding vector distribution at a frequency of 124·1 Hz. This coincides with the third natural frequency of the system and is associated with two bending waves in the x direction and one bending wave in the y direction of each plate. Figure 8 shows findings at a frequency of 201·4 Hz. These correspond to the fifth natural frequency of the system with three bending waves in the x direction and one bending wave in the y direction of each plate. Figure 9 shows results at a frequency of 263·8 Hz. These relate to the seventh natural frequency of the system with one bending wave occurring in the x direction and two bending waves in the y direction.

An L-shaped plate can be separated into two rectangular plates with a time- and frequency-dependent distributed moment excitation applied to the coupling edge of the two plates. This moment excitation together with the angular deformation represent the energy exchange between the two plates. As shown in Figures 7–9, the energy does not always flow simply from source plate (plate I) to receiver plate (plate II), because in some parts along the coupling edge, energy flows from receiver to source plate. The direction of time-averaged

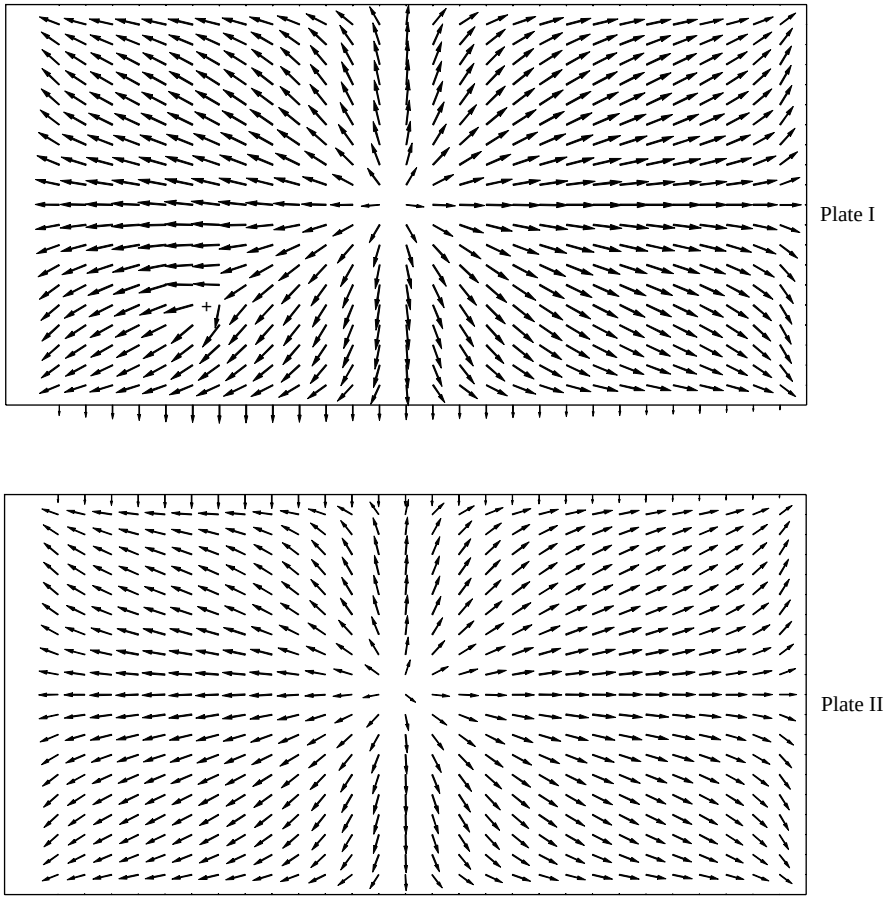

Figure 12. Instantaneous power flow density vector at $f = 77{\cdot}7$ Hz, $t = T/8$. " + " indicates the excitation position.

power flow is dependent on the phase angle between internal force and velocity response. This is demonstrated in Figure 10 through illustration of the shapes of instantaneous bending moment, angular velocity and power flow occurring along the coupling edge of plate I at a frequency of 124·1 Hz. At any position on the coupling edge, when the phase angle between internal bending moment and angular velocity is less than 90°, the sign of the instantaneous power flow is negative and the direction of the rate of energy flow in a period is in a direction indicating energy absorption. Alternatively, if the phase angle is between 90 and 180°, the sign of the instantaneous power flow is positive and the direction of the rate of energy flow in a period is in a direction indicating an output of energy. The total power flowing in and out of the coupling edge remains balanced regardless of the number of plates combining at the coupling edge when the coupling is conservative. This is a mechanism similar to the one observed in Kirchhoff's law of electric current in that the summation of current flow into and out of a connection point is equal to zero.

Power flow in an L-shaped plate under a single force excitation is very complex and frequency dependent. The power flow density at a position near to the source is not necessarily always larger than its density at positions further away from the source. Power flows from the excitation source and usually ends at a boundary but there exists the possibility that the time-averaged power flow density is equal to zero at positions in the

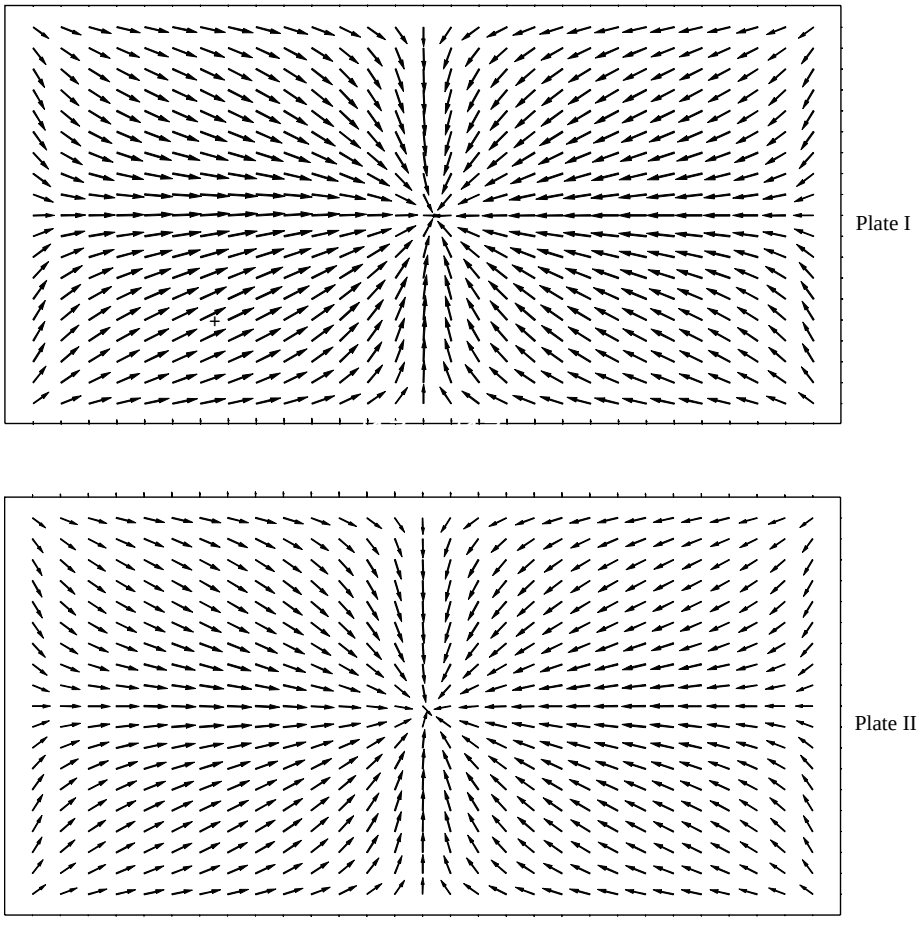

Figure 13. Instantaneous power flow density vector at $f = 77{\cdot}7$ Hz, $t = T/4$. " + " indicates the excitation position.

plate and a circulation- or vortex-type flow exists in the vicinity of this position. Such flows are illustrated in Figures 7–9.

One difficulty encountered in general modal superposition is the convergence of the summation process. Compared to the displacement response, convergence of the calculated internal force (moment and shear force) is poor, especially for the shear force, and therefore a large number of modes are used. The power flow density vector in the plate contains components of both bending moment and shear force, so its convergence is also poor and has the same level of difficulty of calculation as in the shear force case. In the theoretical substructure approach adopted here, such difficulties and effort of computation do not arise because modes and internal forces have formulated expressions. The highest eigenfrequency admitted in the present calculation for a suitable accuracy of convergence of solution in the analysis is at least 500 kHz.

Figures 11–14 illustrate the instantaneous power flow density vector at four different time instants of the first natural frequency at 77·7 Hz. The instantaneous power flow displays the characteristics of energy exchange between kinetic and potential energies. At instants $t = 0$ and $T/8$ (Figures 11 and 12), both plates release energy and it is usual for power to flow from the peak value position of a modal shape to a boundary (i.e., the zero position of a modal

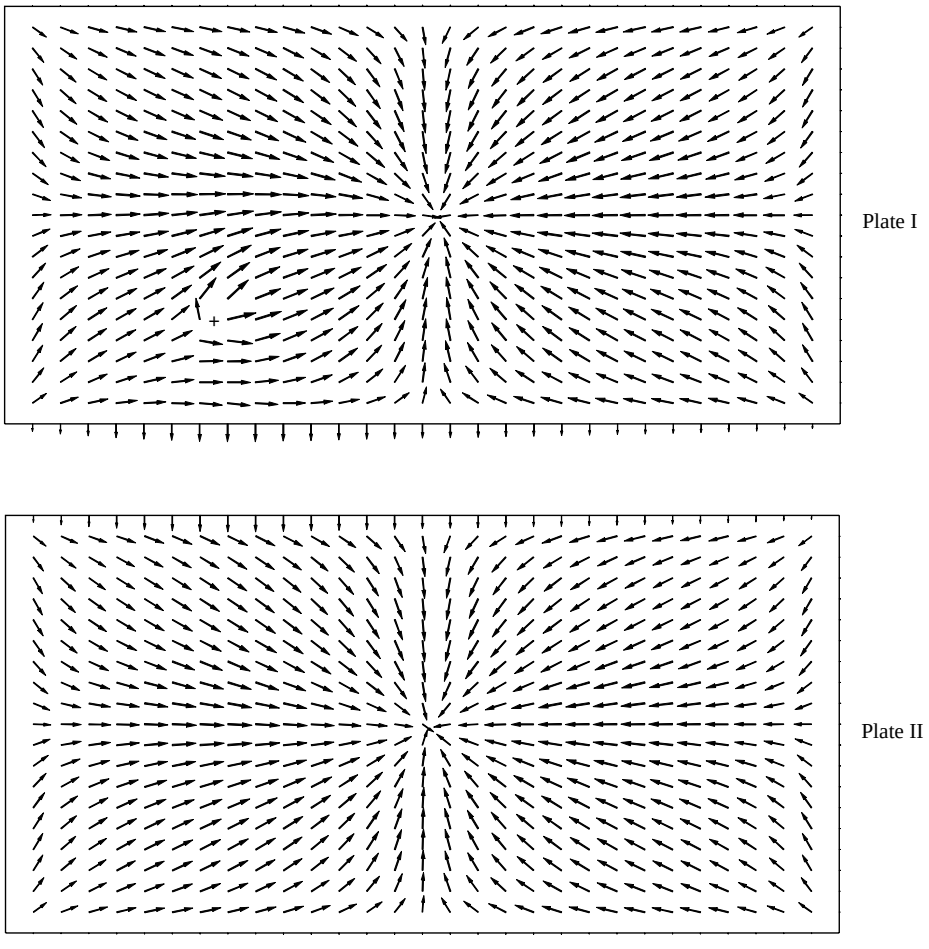

Figure 14. Instantaneous power flow density vector at $f = 77{\cdot}7$ Hz, $t = 3T/8$. " + " indicates the excitation position.

shape). This peak value position acts similar to a power source. At instants $t = T/4$ and $3T/8$ (Figures 13 and 14), both plates absorb energy and there is no obvious power source. Power flows from boundary to the peak value position of the modal shape and this latter position behaves similar to a sink.

3.2.2. *Rigidly connected coupling edge*

Figures 15 and 16 illustrate the variation of the time-averaged transmitted power flows with frequency to different assumed boundary conditions at the coupling edge. An excitation is applied at the centre of plate I and results are presented over the frequency range of 0–1500 Hz (Figure 15) and 2000–4000 Hz (Figure 16). The conditions at the coupling edge are: simply supported (i.e., the same as considered in Figures 4 and 5) and rigidly connected with plates at 45, 90, 135 and 165° to one another. Below 600 Hz, the results derived for all conditions are almost identical. The right angle set of predictions is similar to the simply supported case below the frequency of 4000 Hz which is about 0·7 times the value of the first natural frequency of an in-plane vibration. This implies that the

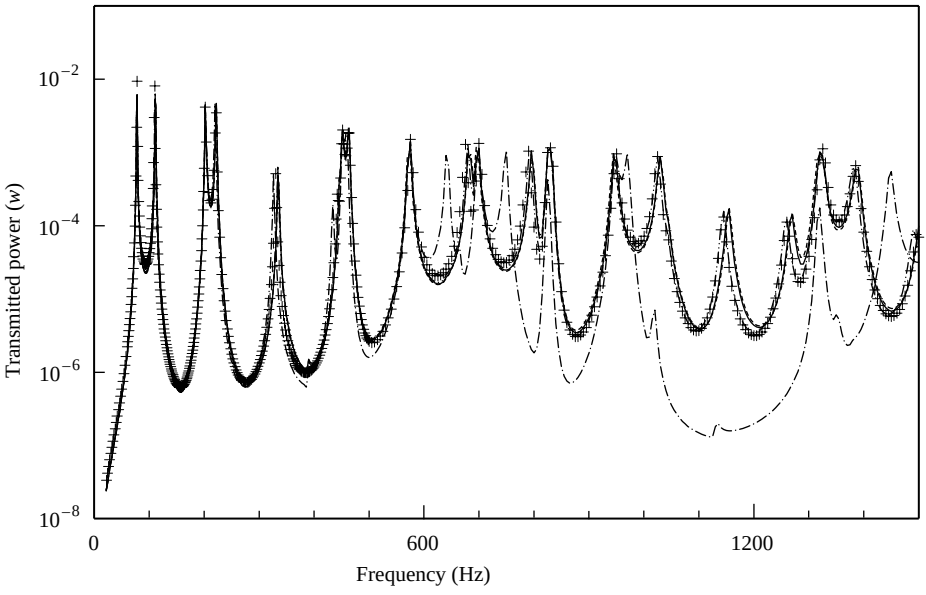

Figure 15. The variation with frequency of time-averaged transmitted power for different coupling angle (0–1500 Hz): +, simply supported; ——, 90°; – – –, 45°; – – – –, 135°; – – – -, 165°.

simply supported case assumption at the right angle coupling edge is valid below a frequency of 0·7 times the value of the first natural frequency of in-plane vibration. The influence of in-plane vibration increases as the angle between the two plates deviates from a right angle.

4. CONCLUSION

Based on the concept of the power flow density vector and its time-averaged value (or structural intensity) in a continuum, a dynamic substructure approach is used to derive the power flow density vector of an L-shaped plate system by combining the force balance and geometrically compatible conditions at the coupled edge. The power flow characteristics of the system are examined numerically. The proposed method can calculate the higher modes easily and efficiently to ensure convergence of solution as well as readily taking into account variations in substructure damping.

On the coupling edge of the L-shaped plate, energy does not always flow from source (plate I) to receiver (plate II) for in some portion of the coupling edge, energy flows from receiver to source plate. The direction of time-averaged power flow is dependent on the phase angle between internal force and velocity response. At positions on the coupling edge where the phase angle between internal bending moment and angular velocity is $< 90°$, the plate absorbs energy. Otherwise, the plate transmits energy when the phase angle is $> 90°$.

The time-averaged power flow density value at positions near the source is not necessarily larger than its value in positions far from the source. Time-averaged power usually flows from the excitation source and ends at a boundary but there is every likelihood that the time-averaged power flow density is equal to zero at positions on the plate and a circulation- or vortex-like structure may exist around this zero density power flow position. The instantaneous power flow describes the characteristics of energy

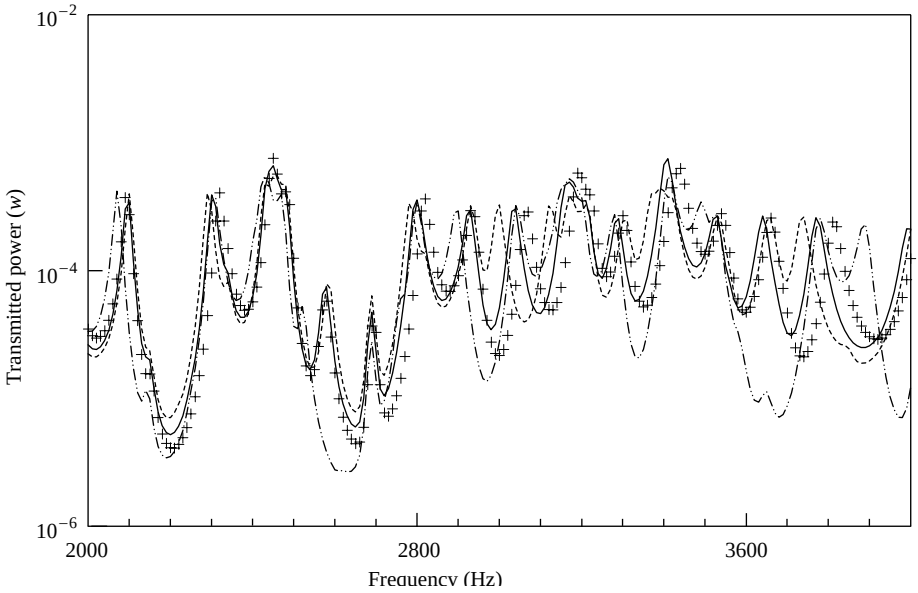

Figure 16. The variation with frequency of time-averaged transmitted power for different coupling angle (2000–4000 Hz): + , simply supported; ——, 90°; – – –, 45°; – – – –, 135°; – – – –, 165°.

exchange between kinetic and potential energy. The peak value position of the modal shape is similar to a power source when the system releases energy and a sink when the system absorbs energy.

In the future, it is planned to complement this study by measuring power flows and structural intensities in simple structures. This investigation provides the mechanisms to measure the relevant parameters.

REFERENCES

1. R. H. LYON 1975 *Statistical Energy Analysis of Dynamic Systems, Theory and Applications.* Cambridge, Massachusetts: MIT Press.
2. R. S. LANGLEY 1990 *Journal of Sound and Vibration* **159**, 483–502. A derivation of the loss factors used in statistical energy analysis.
3. J. E. MANNING 1994 *Philosophical Transactions of Royal Society, London* A **346**, 477–488. Formulation of SEA parameters using mobility functions.
4. H. G. D. GOYDER and R. G. WHITE 1980 *Journal of Sound and Vibration* **68**, 59–75. Vibrational power flow from machines into build-up structures. I. Introduction and approximate analysis of beam and plate-like foundations.
5. H. G. D. GOYDER and R. G. WHITE 1980 *Journal of Sound and Vibration* **68**, 77–95. Vibrational power flow from machines into build-up structures. II. Wave propagation and power flow in beam-stiffened plates.
6. H. G. D. GOYDER and R. G. WHITE 1980 *Journal of Sound and Vibration* **68**, 97–117. Vibrational power flow from machines into build-up structures. III. Power flow through isolation system.
7. J. M. CUSCHIERI 1990 *Journal of the Acoustics Society of America* **87**, 1159–1165. Structural power-flow analysis using a mobility approach of an L-shape plate.
8. R. S. LANGLEY 1989 *Journal of Sound and Vibration* **135**, 319–331. Application of the dynamic stiffness method to the free and force vibrations of aircraft panels.
9. D. W. MILLER and A. VON FLOTOW 1989 *Journal of Sound and Vibration* **128**, 145–162. A travelling wave approach to power flow in structure networks.

10. J. L. HORNER and R. G. WHITE 1991 *Journal of Sound and Vibration* **147**, 87–103. Prediction of vibration power transmission through bends and joints in beam-like structures.
11. L. S. BEALE and M. L. ACCORSI 1995 *Journal of Sound and Vibration* **185**, 685–702. Power flow in two and three dimensional frame structures.
12. Y. P. XIONG, J. T. XING and W. G. PRICE 2001 *Journal of Sound and Vibration* **239**, 275–295. Power flow analysis of complex coupled systems by progressive approaches.
13. Z. H. WANG, J. T. XING and W. G. PRICE *Journal of Sound and Vibration* **249**, 3–22. Power flow analysis of rod/beam systems using a substructure method.
14. H. FARAG and J. PAN 1998 *Journal of the Acoustics Society of America* **104**, 204–216. On the free and forced vibration of single and coupled rectangular plates.
15. M. BESHARA and A. J. KEANE 1998 *Journal of Sound and Vibration* **213**, 511–535. Vibrational energy flows between plates with compliant and dissipative couplings.
16. D. J. NEFSKE and S. H. SUNG 1987 *Statistical Energy Analysis, American Society of Mechanical Engineers*, **NCA-3**, 47–54. Power flow element analysis of dynamic system: basic theory and application to beam.
17. J. C. WOHLEVER and R. J. BERNHARD 1992 *Journal of Sound and Vibration* **153**, 1–19. Mechanical energy flow models of rods and beams.
18. C. SIMMONS 1990 *Journal of Sound and Vibration* **144**, 215–227. Structure-borne sound transmission through plate junctions and estimates of SEA coupling loss factors using the FE method.
19. G. STIMPSON and N. LALOR 1992 *Internoise* **92**, 557–560. SEA extension of a F. E. model to predict total engine noise.
20. J. A. STEEL and R. J. M. CRAIK 1993 *Journal of Sound and Vibration* **178**, 553–561. Statistical energy analysis of structure-borne sound transmission by finite element methods.
21. C. R. FREDO 1992 *Journal of Sound and Vibration* **199**, 645–666. SEA-like approach for the derivation of energy flow coefficients with a finite element model.
22. B. R. MACE and P. J. SHORTER 2000 *Journal of Sound and Vibration* **233**, 369–389. Energy flow models from finite element analysis.
23. K. SHANKAR and A. J. KEANE 1995 *Journal of Sound and Vibration* **185**, 867–890. Energy flow prediction in a structure of rigidly joined beams using receptance theory.
24. K. SHANKAR and A. J. KEANE 1997 *Journal of Sound and Vibration* **201**, 491–513. Vibrational energy flow analysis using a substructure approach: the application of receptance theory to FEA and SEA.
25. S. A. HAMBRIC 1990 *Journal of Vibration and Acoustics* **112**, 542–549. Power flow and mechanical intensity calculations in structural finite element analysis.
26. L. GAVIC and G. PAVIC 1993 *Journal of Vibration and Acoustics* **164**, 29–43. A finite element method for computation of structural intensity by the normal mode approach.
27. J. T. XING and W. G. PRICE 1999 *Proceeding of the Royal Society* A **455**, 401–436. A power-flow analysis based on continuum dynamics.
28. J. PAN and C. H. HANSEN 1991 *Journal of the Acoustics Society of America* **89**, 200–209. Active control of total vibratory power flow in a beam. I: Physical system analysis.
29. A. LEISSA 1993 *Vibration of Plates*. Woodbury, New York: Acoustical Society of America.
30. H. REISMANN and P. S. PAWLIK 1980 *Elasticity Theory and Application*. New York: Quantum.
31. D. J. GORMAN 1982 *Free Vibration Analysis of Rectangular Plates*. New York: Elsevier.
32. LORD RAYLEIGH 1894 *Theory of Sound*. London: Macmillan.
33. L. CREMER, M. HECKL and E. E. UNGAR 1988 *Structure-borne Sound*. Berlin: Springer-Verlag.
34. R. M. GRICE and R. J. PINNINGTON 2000 *Journal of Sound and Vibration* **232**, 449–471. Vibration analysis of a thin-plate box using a finite element which accommodates only in-plane motion.
35. F. J. FAHY 1989 *Sound Intensity*. London: Elsevier Science Publishers.
36. J. T. XING, W. G. PRICE and Q. H. DU 1996 *Philosophical Transactions of Royal Society, London* A **354**, 259–295. Mixed finite element substructure–subdomain methods for the dynamic analysis of coupled fluid–solid interaction problems.

APPENDIX A: NOMENCLATURE

a, b	length and width of rectangular plate
C_L	longitudinal wave speed
C_T	transverse (in-plane) shear wave speed

D	plate flexural rigidity
E	Young's modulus
$\mathbf{f}(t)$	general expression of exciting forces
$[\mathbf{f}_j^e]$, $[\mathbf{f}_j^c]$	external excitation and internal coupling force matrixes on the jth plate respectively
h	thickness of plate
i	$=\sqrt{-1}$
m_{rp}	generalized modal mass
M_{xx}, M_{yy}, M_{xy}	internal bending moments and twisting moment per unit length
$[\mathbf{M}b_j^e]$, $[\mathbf{M}b_j^c]$	receptance functions between displacements at coupling edges and external excitations or internal coupling forces of the jth plate
n	mode number used in modal analysis
N_{yy}	internal in-plane longitudinal force
$P_{rp}(t)$	principal co-ordinate
Q_x, Q_y	transverse shearing forces per unit length
q	general expression for power flow
$\langle q \rangle$	general expression for time-averaged power flow
T	a period of excitation
$[\mathbf{T}]$	orthogonal transformation matrix between global and local co-ordinate systems
$[\mathbf{U}_j^c]$	displacement matrix at the coupling edge of plate j
$v(t)$	general expression for transverse velocity
$w(t)$	general expression for displacement
x, y, z	spatial co-ordinates
α	the angle between global and local co-ordinate systems
$\delta(x)$	Dirac delta function
η	damping loss factor
λ_r	eigenvalue ($=\omega_r a^2\sqrt{\rho / D}$)
φ_v	general expression for phase angle
φ_r, φ_{rp}	principal mode shape
ϕ	plate aspect ratio
μ	the Poisson ratio
θ	general expression for slope angle
ρ	mass density
$\boldsymbol{\sigma}_{ij}$	stress tensor
ω	exciting frequency
ω_{rp}	natural frequency
$[\ ]^{\mathrm{T}}$	transpose of a matrix
$[\ ]^{-1}$	an inverse matrix
(*)	conjugate of a complex variable